

Article

Highly Enhancing the Interfacial and Mechanical Properties of Basalt Fiber/Poly(phthalazinone ether nitrile ketone) Composite by Thermoplastic Sizing Agents with Different Structures

Hang Jia ^{1,2}, Cheng Liu ^{1,2,3,*} , Yue Qiao ^{1,2}, Yu Zhang ^{1,2}, Kaiyuan Fan ¹, Manxia Zhang ⁴ and Xigao Jian ^{1,2,3}

¹ State Key Laboratory of Fine Chemicals, Dalian University of Technology, Dalian 116024, China; POLYJH@mail.dlut.edu.cn (H.J.); qiao123@mail.dlut.edu.cn (Y.Q.); zhangyu25@mail.dlut.edu.cn (Y.Z.); 18266003166@mail.dlut.edu.cn (K.F.); jian4616@dlut.edu.cn (X.J.)

² Department of Polymer Science & Materials, Dalian University of Technology, Dalian 116024, China

³ Dalian Basalt Fiber Resin Matrix Composite Engineering Research Center, Dalian 116012, China

⁴ Department of Environmental Science & Engineering, Dalian Maritime University, Dalian 116026, China; zhangmanxia@163.com

* Correspondence: liuch1115@dlut.edu.cn; Tel.: +86-411-84986191

Abstract: The interfacial modification of basalt-fiber-reinforced polymer (BFRP) composites is an essential research field and many techniques have been developed to improve the adhesion between basalt fiber (BF) and the matrix. However, most studies were based on the matrixes of general plastics and epoxy resins. In this work, five different chain structures of thermoplastic sizing agents were used to improve the interfacial properties of unidirectional BF-reinforced soluble and high-temperature-resistant poly(phthalazinone ether nitrile ketone) (BF/PPENK) composites. DMA results showed that the poly(ether nitrile) (PEN)-sized BF/PPENK (BF-PEN/PPENK) composite exhibited the optimal interfacial performance, with a storage modulus (E') and glass transition temperature (T_g) up to 50 GPa and 288 °C, respectively. Moreover, the tensile strength, compressive strength, flexural strength, and interlaminar shear strength of the BF-PEN/PPENK composite reached 778 MPa, 600 MPa, 1115 MPa and 57 MPa, respectively, and increased by 42%, 49%, 20% and 30% compared with the desized BF/PPENK composite. This study provides some suggestions for the design of sizing agents to modify the interface of BF and high-performance thermoplastic resin.

Keywords: basalt fiber; high-performance thermoplastic resin; composite; interfacial modification



Citation: Jia, H.; Liu, C.; Qiao, Y.; Zhang, Y.; Fan, K.; Zhang, M.; Jian, X. Highly Enhancing the Interfacial and Mechanical Properties of Basalt Fiber/Poly(phthalazinone ether nitrile ketone) Composite by Thermoplastic Sizing Agents with Different Structures. *Polymers* **2022**, *14*, 2947. <https://doi.org/10.3390/polym14142947>

Academic Editor: Bon-Cheol Ku

Received: 6 June 2022

Accepted: 15 July 2022

Published: 21 July 2022

Publisher's Note: MDPI stays neutral with regard to jurisdictional claims in published maps and institutional affiliations.



Copyright: © 2022 by the authors. Licensee MDPI, Basel, Switzerland. This article is an open access article distributed under the terms and conditions of the Creative Commons Attribution (CC BY) license (<https://creativecommons.org/licenses/by/4.0/>).

1. Introduction

Fiber-reinforced polymer (FRP) composites, such as carbon fiber [1], glass fiber [2], aramid fiber [3], ultra-high-molecular-weight polyethylene fiber [4], polypropylene fiber [5] and basalt fiber [6], etc., have obtained wide range of applications for their light weight, high strength, impact resistance, corrosion resistance. In particular, basalt fiber (BF) possesses some favorable properties, such as non-pollution, low cost, high- and low-temperature resistance, chemical stability, thermal insulation, sound absorption, and flame-retardant nature, and especially excellent mechanical properties [7–11]. Basalt-fiber-reinforced polymer (BFRP) composites, combining the advantages of the fiber and resin, have great potential in the fields of building, aerospace, petrochemical, automobile, marine, energy conservation, and environmental protection [12–15]. However, the surface of BF is quite smooth and inert, and the interfacial adhesion between the fiber and resin is weak [16–18]. Therefore, various strategies have been used to construct a reasonable interfacial structure of the BFRP composites to improve their interfacial performance.

The sizing treatment of the fiber surface is a simple, easy-to-operate and industrialized strategy, which mainly includes silane coupling-agent modification, polymer sizing, nanoparticle adhesion, etc. [19–21]. Among them, polymer sizing has been regarded as

a standardized and commercially available method of fiber surface treatment during the manufacturing process of commercial fibers [22], due to its advantages of preventing the fluffs and yarn breakage without damaging the surface and properties of fibers [23–25]. However, most commercial polymer sizing agents are variously diluted epoxy resins, whose degradation temperatures (about 250 °C) are much lower than the processing temperatures of high-performance engineering plastics [26–28]. This would inevitably result in the degradation of the polymer coating on the fiber surface under the high temperature of composite processing and, thus, the defects on the interface of the fiber and heat-resistant thermoplastic resin [29]. Furthermore, the compatibility between the epoxy thermoset (TS) resin and heat-resistant thermoplastic (TP) matrix is not very high, which has a passive effect on the interfacial properties of composites. Therefore, the design and synthesis of heat-resistant thermoplastic sizing agents are particularly important for the development and application of high-performance thermoplastic polymer composites.

The polymer sizing agents generally used are polymers with relatively low molecular weight (LMW), and their modulus is lower than that of the fiber and matrix. According to the “deformation layer theory” [30], if the polymer sizing agent has good compatibility with the resin matrix, it will form an interfacial deformation layer to better buffer the direct stress impact on the fibers. Therefore, considering the high-temperature processing of fiber-reinforced high-performance thermoplastic polymer (FRHTP) composites and the extreme service environment, polymer sizing agents should have the following characteristics: high-temperature resistance, certain compatibility with the matrix, good solubility, or easy dispersibility.

At present, many efforts have been focused on modifying the interface of fiber-reinforced poly(ether ether ketone) (PEEK) composites by designing oligomeric high-performance polymers as sizing agents, which have similar chemical structures and good compatibility to the PEEK matrix. Zhu et al. [31] established an effective interfacial enhancement method for GF/PEEK composites by introducing aminated poly(ether ether ketone) on the surface of the glass fibers. Wang et al. [32] and Hassan et al. [33] reported a transformed fiber surface morphology and chemical composition with heterocyclic poly(aryl indole ketone) and soluble poly(ether ketone ketone) separately, to improve the interfacial properties of CF/PEEK composites. Wang et al. [34] used polyimide (PI) to modify the surface of short carbon fibers (SCF), and the tensile strength and bending strength of PI-coated SCF/PEEK composites showed improvements of 11.8% and 16.6%, respectively, compared with commercial cases. However, these modification methods all require the pre-activation of the fibers, which inevitably causes the fibers to be damaged, and the synthesis and treating processes are also complicated.

In addition, until now, there are still very few reports on the interfacial properties of basalt-fiber-reinforced high-performance thermoplastic polymer (BFRHTP) composites, which hinders the application and development of basalt fiber in high-end manufacturing industries. This may be because of the smoother and more inert surface of BF compared with CF, and the difficulty of balancing its surface activation and fiber strength. Therefore, it is significant to explore the influence of structures of polymer sizing agents on the interfacial properties of BFRHTP composites.

In this work, five low-molecular-weight (LMW) thermoplastic polymers ($\bar{M}_n = 10,000$ g/mol), namely polyvinylpyrrolidone (PVP), polyether nitrile (PEN), poly(phthalazinone ether ketone) (PPEK), poly(phthalazinone ether nitrile) (PPEN), and poly(phthalazinone ether nitrile ketone) (PPENK), were used as sizing agents for the surface treatment of basalt fibers. The chains of PEN, PPEK, PPENK, and PPEN have aromatic rigid structures, which are similar to the matrix, but their cyano group content and flexibility of them are different. Additionally, PVP with an aliphatic structure has better flexibility than the other four sizing agents. Then, the effect of the chain structures of the sizing agent on the

interfacial and mechanical properties of BF/PPENK composites was investigated in detail. Furthermore, the solubility parameters of the sizing agents and the PPENK matrix resin were calculated by the group contribution method, and their compatibilities were analyzed by these parameters. XPS and SEM were used to characterize the chemical composition and morphology of the BF surfaces, respectively. The dynamic thermomechanical analysis (DMA) was performed to reveal the thermal property and interfacial adhesion of the BF/PPENK composites. A tensile test, compression test, bending test, and interlayer shear test were employed to evaluate the mechanical properties of the BF/PPENK composites. The failure modes and mechanisms of the tensile and compression test were analyzed by the optical microscope and SEM. This study provides some suggestions for the design of sizing agents to modify the interface of BF and high-performance thermoplastic resin.

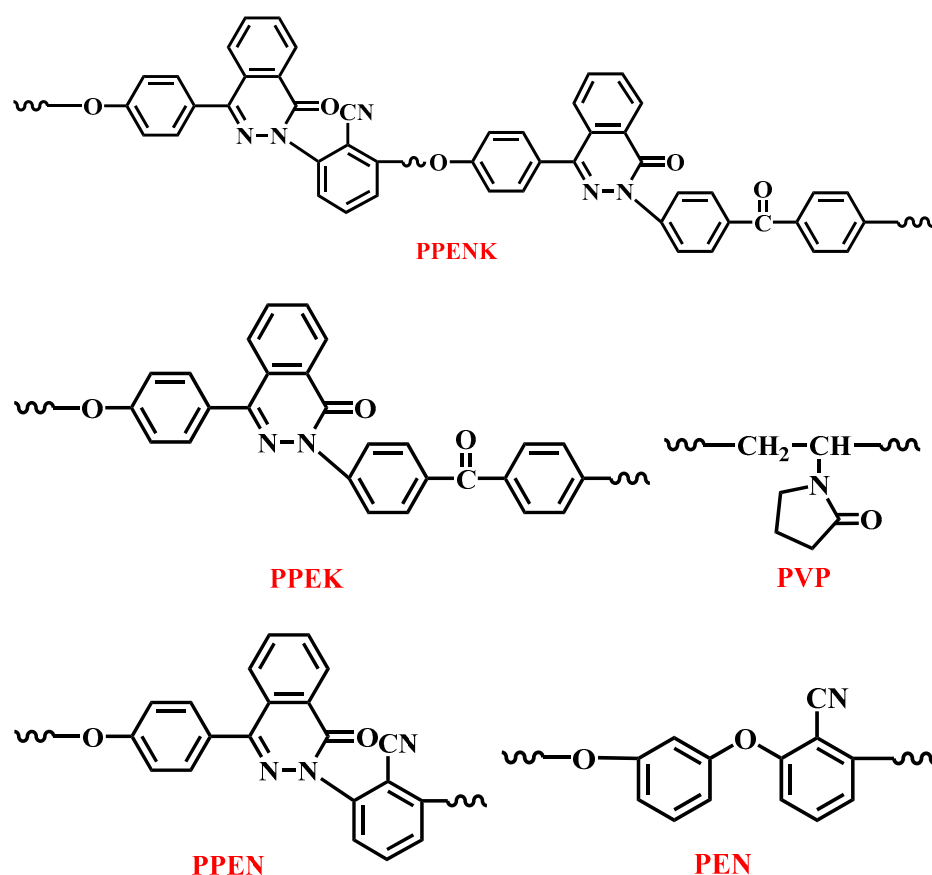
2. Materials and Experiments

2.1. Materials

Continuous basalt fiber (untwisted roving; diameter, 9 μm ; density, 2.8 g/cm^3 ; tensile strength and modulus, 2.3 GPa and 84 GPa, respectively) was kindly provided by Guizhou Shixin Basalt Technology Co., Ltd., Guiyang, China. Poly(phthalazinone ether nitrile ketone) (PPENK, nitrile: ketone, 1:1; intrinsic viscosity, 0.44 dL/g) resin and 4-(4-hydroxyphenyl)phthalazinone (DHPZ) were purchased from Dalian Polymer New Material Co., Ltd., Dalian, China. 1,3-Dihydroxybenzene (DHB), 2,6-difluorobenzonitrile (DFBN), 4,4'-difluorophenyl ketone (DFK) and polyvinylpyrrolidone (PVP, K13–18, $\approx 10,000$ g/mol) were obtained by Shanghai Aladdin Bio-Chem Technology Co., Ltd., China. Anhydrous potassium carbonate (K_2CO_3), *N,N*-dimethylacetamide (DMAc), *N*-methylpyrrolidone (NMP), toluene, ethanol, and acetone were obtained from Sinopharm Chemical Reagent Co., Ltd., Shanghai, China and used directly without any treatment.

2.2. Synthesis of the TP Sizing Agents

The chemical structures of PPENK, PPEK, PVP, PPEN and PEN are exhibited in Scheme 1, and their 5% thermal-decomposition temperatures are shown in Figure S1, which all meet the processing requirement. The number-average molecular weight of the designed polymers was 10,000 g/mol , with a theoretical DP of 49, 53, 63, 95 and 103 for PPEK, PPENK, PPEN, PEN and PVP, respectively. Except for PVP, the other four LMW sizing agents, PPEK, PPEN, PPENK (N:K = 1:1) and PEN, were synthesized according to the similar procedure in our previous works [35,36]. Taking the LMW PEN, for instance, a typical principle of polymerization was performed as shown in Figure S2. DHB (0.09792 mol, 10.9667 g), DFBN (0.1 mol, 13.9110 g), anhydrous K_2CO_3 (0.14 mol, 19.3494 g), 25 mL NMP and 45 mL toluene were added to a 250 mL three-necked round-bottom flask outfitted with a mechanical stirrer, a nitrogen inlet, a Dean–Stark trap outfitted with a condenser, and a nitrogen inlet and outlet. Firstly, the mixture was stirred at 130 $^\circ\text{C}$ for 2 h under an N_2 atmosphere to distill the resultant water azeotropically, and then the toluene was distilled off. Subsequently, the mixture was stirred at 160 $^\circ\text{C}$ for 8 h. The resultant viscous mixture was poured into hot deionized water with vigorous stirring, and the precipitated product was rinsed with hot deionized water three times, and then dried under a vacuum at 120 $^\circ\text{C}$ for 24 h.



Scheme 1. Chemical structures of PPENK, PPEK, PVP, PPEN and PEN.

2.3. Preparation of Composites

Acetone was used to remove the pristine sizing and pollutants on the surface of BFs for 48 h [37]. Then, they were cleaned with deionized water and dried in a vacuum oven at 120 °C for 4 h to obtain the desired BF. The LMW PVP, PEN, PPEK, PPEN and PPENK were separately dispersed in NMP, and the ratio of solid to solvent was 1 g/100 mL. Then, after ultrasonication (5 min), standing (15 min) and drying (150 °C, 30 min), the desired BFs were covered with LMW polymer coating, named BF-PVP, BF-PEN, BF-PPEK, BF-PPEN and BF-PPENK, respectively. The resized BFs were placed in a dipping tank (the ratio of solute mass to solvent volume is 0.16 g/mL), and the BF/PPENK prepreps were prepared by the solution dipping method. Finally, the dried prepreps were cut into a suitable size, and the unidirectional composite laminates were prepared through a vacuum thermocompression up to 320 °C with a pressure of 7 MPa (as is shown in Figure S3), named BF-PVP/PPENK, BF-PEN/PPENK, BF-PPEK/PPENK, BF-PPEN/PPENK and BF-PPENK/PPENK, respectively. The volume fraction of BFs in the BF/PPENK composites was about 43% (mass fraction was about 60%).

2.4. Characterization

X-ray photoelectron spectroscopy (XPS, ESCALAB250Xi; optimum sensitivity: 1,000,000 cps (Mono XPS, Ag 3d5/2)) was used to characterize the surface chemical element compositions of different surfaces of the modified BF. Scanning electron microscopy (SEM, SU8200; loading voltage and current: 5 kV and 10 μA; SEI resolution ratio: 0.8 nm) was employed to investigate the microscopic surface of BFs and the fracture morphologies of BF/PPENK composites after the tensile test and compression test. The optical microscope (Nikon, ECLIPSE LV100ND) was used to observe the side of the polished compressive failing sample and study its failing mode (the magnification was 50 times).

The thermal stability of the sizing agents was measured by thermal gravimetric analysis (TGA, METTLER TOLEDO TGA1) at a heating rate of 20 °C/min from 30 °C to 800 °C (after being kept at 150 °C for 10 min) under a nitrogen atmosphere. Dynamic mechanical analysis (DMA, sample size: 40 × 6 × 2 mm³) measurement was carried out on METTLER TOLEDO DMA/SDTA861e at a single cantilever clamp, 1 Hz, 3 N, and a heating rate of 3 °C/min, from 30 °C to 350 °C under air atmosphere.

Tensile test (sample size: 250 × 15 × 1.5 mm³), compression test (sample size: 80 × 12.5 × 2 mm³), flexural test (sample size: 80 × 12.7 × 2 mm³), and interlaminar shear strength test (sample size: 20 × 10 × 2 mm³) of the BF/PPENK composites were determined on a universal testing machine (Instron 5982; 100 kN force sensor) according to ASTM D3039, SACMA SRM 1R, ASTM D790 and ISO 14130, respectively. At least five parallel measurements were conducted and averaged for each final result.

3. Results and Discussion

3.1. Compatibility of Polymer Sizing Agents and PPENK Matrix

The group contribution method was used to calculate the solubility parameters of LMW PVP, PEN, PPEK, PPEN and PPENK. The results of solubility parameters and their different components are shown in Table 1. According to the principle of similar solubility parameters, we compared the differences in total solubility parameters ($|\delta_t - \delta_{t,matrix}|$) between each polymer sizing agent and matrix resin ($\delta_{t,matrix}$) to preliminarily determine their respective compatibility. The calculation indicated that the $|\delta_t - \delta_{t,matrix}|$ of PVP, PEN, PPEK, PPEN and PPENK are 0.58, 0.28, 0.26, 0.35 and 0, respectively. These differences are very small, indicating the good compatibility between these sizing agents and the PPENK matrix, and further sorting the compatible degree of them obtained the order PPENK > PPEK > PEN > PPEN > PVP. However, the differences in polarization components ($|\delta_p - \delta_{p,matrix}|$) between the PVP, PEN, PPEK, PPEN and PPENK and the matrix are 5.35, 1.34, 0.8, 0.95 and 0, respectively. According to the “similar polarity principle” and “structural similarity principle”, the compatibility of PEN with the matrix is weaker than PPEN. Therefore, the final compatible degree of them is PPENK > PPEK > PPEN > PEN > PVP.

Table 1. Solubility parameter values of the PPENK matrix resin and sizing agents ^a.

Sample	δ_d	δ_p	δ_h	δ_t	$ \delta_t - \delta_{t,matrix} $	$ \delta_p - \delta_{p,matrix} $
PPEK	19.51	5.02	6.83	21.27	0.26	0.8
PPENK	19.44	5.82	7.21	21.53	0	0
PPEN	19.35	6.77	7.65	21.88	0.35	0.95
PVP	16.98	11.35	8.46	22.11	0.58	5.53
PEN	19.82	7.16	5.62	21.81	0.28	1.34

^a where δ_t , δ_d , δ_p and δ_h represent the total solubility parameter, dispersion component, polarization component and hydrogen bond component, respectively.

3.2. The Surface Morphology and Elements of BFs

SEM images for the BFs treated with different sizing agents are shown in Figure 1. The surface of the desized BF treated with acetone is considerably smooth (Figure 1a), and it is chemically inert and cannot form chemical bonds with the polymer matrix. Therefore, the BFs without any surface treatment have difficulty in forming a dependable interfacial phase with PPENK. As illustrated in Figure 1b–f, the surface morphologies of the resized BFs are much rougher than the BF—desized. Furthermore, their roughness and morphology are different, which can be attributed to the film-forming capacity of these TP sizing agents on the BF surface. According to the morphologies of the resized BF surfaces, the uniformity, smoothness and integrity were used as the criteria for judging the film-forming ability, in the order of PVP > PEN > PPEN > PPEK > PPENK. This may be ascribed to the different flexibility of molecular chains and their adhesion with BF.

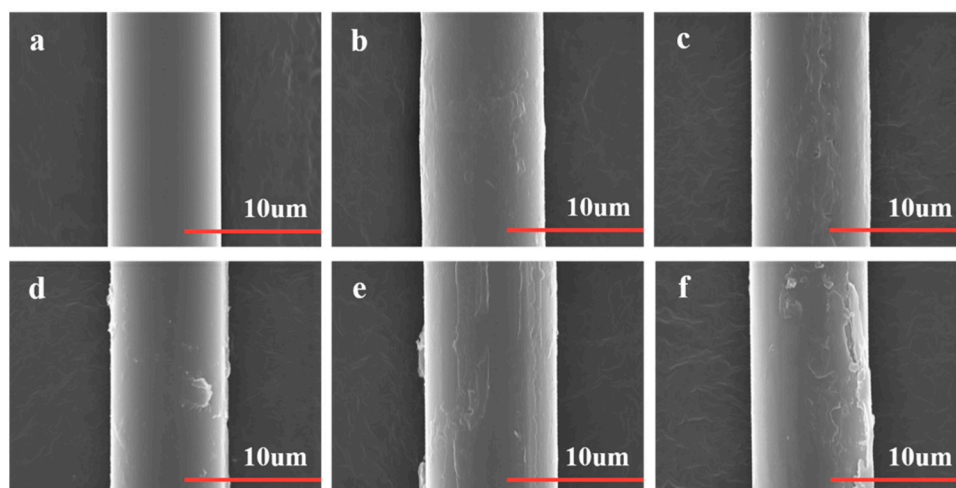


Figure 1. SEM images of (a) BF—Desized, (b) BF-PVP, (c) BF-PEN, (d) BF-PPEK, (e) BF-PPEN and (f) BF-PPENK.

The high-resolution XPS $N(1s)$ peaks for the desized and resized BFs are shown in Figure S4b. It should be noted that the desized BF had only a weak N-H bonding at 399.7 eV [38]. However, the $N(1s)$ peaks of BF-PVP were deconvoluted into two specific peaks at 399.4 eV (pyrrolic N) and 400.1 eV (O=C-N). Additionally, the signal of the C≡N bond at 399.35–399.55 eV appears for BF-PEN, BF-PPEN and BF-PPENK. Furthermore, the characteristic peaks at 399 eV, 399.25–399.95 eV, 399.95–400.8 eV and 400.9–401.9 eV are associated with C-N, N-N, C=N and O=C-N bonds in the phthalazinone structure, respectively. The chemical compositions of $C(1s)$, $O(1s)$, and $N(1s)$ were examined with reference to $Al(2p)$, which is absent in the TP sizing agents. The results indicated that the resized BFs had a higher ratio of O/Al and N/Al compared with the desized BF (Table S2). In particular, the BF-PEN surfaces have the highest contents of N and O elements and polarity, deriving from cyano and ether bonds, because of the high-number-average DP of PEN. Similarly, the high content of N and O elements on the surface of BF-PVP comes from the abundant pyrrolidone rings, also giving it higher polarity. However, the content of N and O elements on the surfaces of BF-PPEK, BF-PPEN and BF-PPENK decreased greatly, which was more related to their low-number-average DP. Therefore, combined with the SEM results, five sizing agents were successfully coated on the BF surface and showed different surface morphologies and elemental characteristics.

3.3. Interfacial Properties

The loss factor ($\tan\delta$) is defined as the ratio of the loss modulus to the storage modulus, and represents the ability of materials to lose energy by alternate load [39] and the peak temperature of the $\tan\delta$ curve is the glass transition temperature (T_g). Moreover, the $\tan\delta$ peak value ($\tan\delta_{max}$) can also be used to evaluate the interfacial adhesion of the resin matrix composites; namely, the lower the $\tan\delta_{max}$ value, the better interfacial adhesion [39,40]. As shown in Figure 2a, except for BF-PVP/PPENK, the $\tan\delta_{max}$ values of the other four sizing-modified BF/PPENK composites were lower than the BF—Desized/PPENK composite, indicating the improved interfacial properties between the resized BFs and the PPENK matrix. Furthermore, the T_g of the BF-PVP/PPENK was increased by 6 °C compared with that of the BF—Desized/PPENK composite, due to the enhanced interfacial properties. Additionally, the increased $\tan\delta_{max}$ for BF-PVP/PPENK may be ascribed to the much lower T_g of interfacial PVP than the PPENK matrix and its higher viscosity at its elastomeric state (285 °C) than other sizing agents with higher T_g , as evidenced by its largest loss modulus and loss factor (Figure S5a). Moreover, the improved mobility of the interfacial layer caused the declined T_g of BF-PPEK/PPENK and BF-PPENK/PPENK composites, which may be related to the low-number-average DP and weak polarity of the sizing agents. Therefore,

the lowest $\tan\delta_{max}$ (0.5559) and the highest T_g (288 °C) demonstrated that PEN was the most effective sizing agent for improving the interfacial phase structure of the BF/PPENK composites than the others (Table S3).

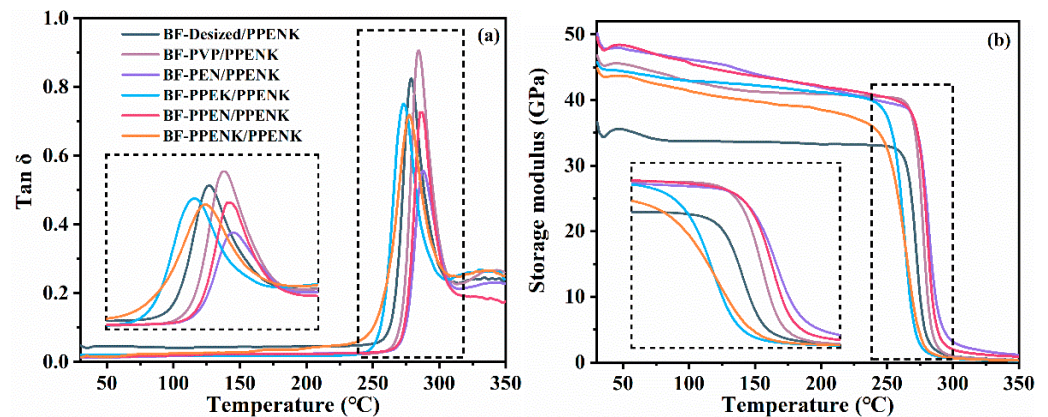


Figure 2. Dynamic thermomechanical analysis of the BF—Desized/PPENK, BF-PVP/PPENK, BF-PEN/PPENK, BF-PPEK/PPENK, BF-PPEN/PPENK and BF-PPENK/PPENK composites; (a) loss factor curves and (b) storage modulus curves.

Moreover, Zorowski and Murayama [41] proposed that the $\tan\delta$ of the composite can be divided into two parts of the energy dissipation at the individual components and the interface. The loss factor of a composite can be stated as:

$$\tan\delta_c = \tan\delta_s + \tan\delta_{in} \quad (1)$$

where $\tan\delta_c$, $\tan\delta_s$ and $\tan\delta_{in}$ are loss factors of the composite, the single component (PPENK and BF) and the interface, respectively.

However, $\tan\delta_{in}$ cannot be measured directly, and can only be calculated by taking the difference between $\tan\delta_c$ and $\tan\delta_s$, so as to further evaluate the interfacial properties of the composite. The $\tan\delta_s$ can be obtained from the complex modulus of the fiber and matrix according to the following formula:

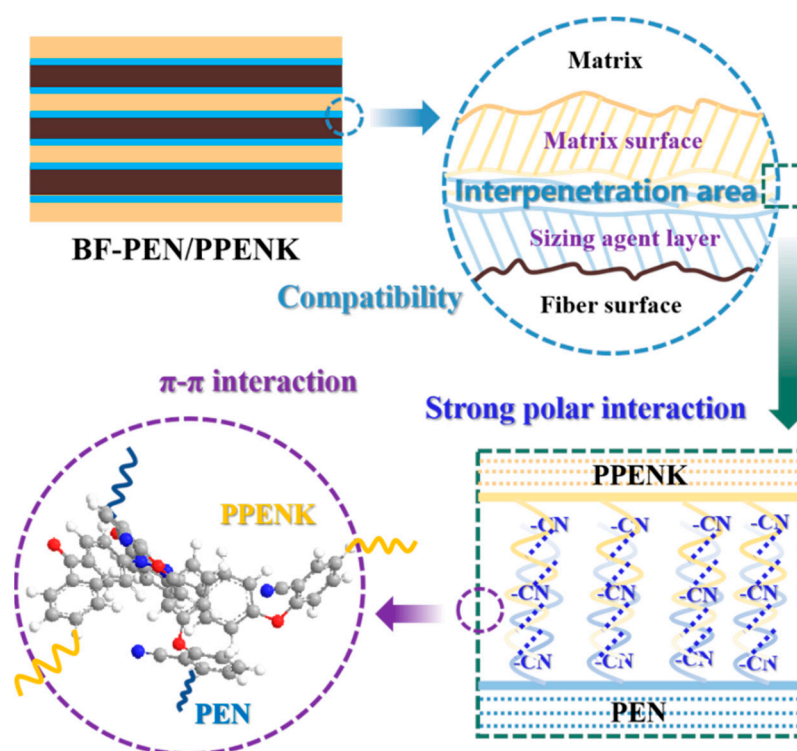
$$\tan\delta_s = \frac{\tan\delta_f \cdot E'_f \cdot V_f}{E'_c} + \frac{\tan\delta_m \cdot E'_m \cdot V_m}{E'_c} \quad (2)$$

where the $\tan\delta_m$, E'_m and V_m are the loss factor, storage modulus and volume fraction of PPENK, and the $\tan\delta_f$, E'_f , and V_f are the loss factor, storage modulus and volume fraction of the BF, respectively.

Compared with the $\tan\delta_m$, the $\tan\delta_f$ would be almost zero, because of the much higher stiffness of BF than the matrix. Therefore, the $\tan\delta_s$ is only determined by the $\tan\delta_m$, E'_m , V_m and E'_c , and the $\tan\delta_{in}$ can be represented by the following formula:

$$\tan\delta_{in} = \tan\delta_c - \frac{\tan\delta_m \cdot E'_m \cdot V_m}{E'_c} \quad (3)$$

The E'_m and $\tan\delta_m$ were measured in our previous work [42], and the $\tan\delta_{in}$ curves are shown in Figure S5b. The lower interfacial loss represents the better interfacial bonding ability of the composite [43]. Therefore, the BF-PEN/PPENK composite may have the highest interfacial bonding strength among these resized BF/PPENK composites. The great improvement in interfacial properties may be attributed to the strong polar interaction, π - π interaction, and good compatibility of the LMW PEN agent and PPENK matrix (Scheme 2).



Scheme 2. Schematic diagram of the PEN sizing agent enhancing the BF/PPENK composite interfacial properties.

Storage modulus (E') is the contribution of the elastic component of composites, and is primarily determined by the matrix, fiber and interfacial adhesion. As the temperature increased, the E' of the BF/PPENK composites decreased slowly before T_g (Figure 2b), because of the relaxation process in the polymer matrix. The initial E' of the BF-PVP/PPENK, BF-PEN/PPENK and BF-PPENK/PPENK composites was 46.78 GPa, 50.14 GPa and 49.50 GPa, which were increased by 27.6%, 36.8% and 35.1% compared with BF—Desized/PPENK (36.65 GPa), respectively, and their E' values were higher than the BF—Desized/PPENK in the whole test temperature range. Additionally, the initial E' of the BF-PPEK/PPENK and BF-PPENK/PPENK composites also reached 45.74 GPa and 44.81 GPa, respectively. However, their E' curves were located below the BF—Desized/PPENK after 250 °C, which is consistent with the results obtained from the $\tan\delta$ curves. In conclusion, constructing a flexible interfacial phase structure for the BF/PPENK composites is a very effective interfacial modification strategy. In addition, combined with the compatibility results, it can be found that the polar interaction plays a more important role than compatibility between the sizing agent and matrix for improving the interfacial properties of BF/PPENK composites.

3.4. Tensile Properties

As illustrated in Figure 3, all the values of tensile strength, modulus and elongation for the resized BF/PPENK composites are much higher than those of the desized BF/PPENK composite (547 MPa, 28 GPa and 2.25%), which may be attributed to the enhanced interfacial adhesion. The BF-PEN/PPENK composite, which has the highest interfacial properties, displayed the tensile strength, modulus and elongation at break of 778 MPa, 33 GPa and 2.87%, about 42%, 18% and 28% higher than those of desized BF/PPENK, respectively. In addition, it is worth mentioning that BF-PVP/PPENK exhibited a high tensile strength, modulus and elongation at break of 751 MPa, 34 GPa and 2.78%, about 37%, 21% and 24%, respectively, which further proved that the flexible interfacial phase can effectively retard the crack propagation and improve the interfacial properties of the composites. Furthermore, as for the other three composites with similar sizing agents containing

a phthalazinone structure, BF-PPEN/PPENK exhibited higher tensile strength, tensile modulus and elongation at break of 722 MPa, 31 GPa and 2.76%, respectively, than those of BF-PPEK/PPENK and BF-PPENK/PPENK. This may be due to the relatively better film-forming properties and more polar cyano groups ($-\text{CN}$) of PPEN than those of PPEK and PPENK.

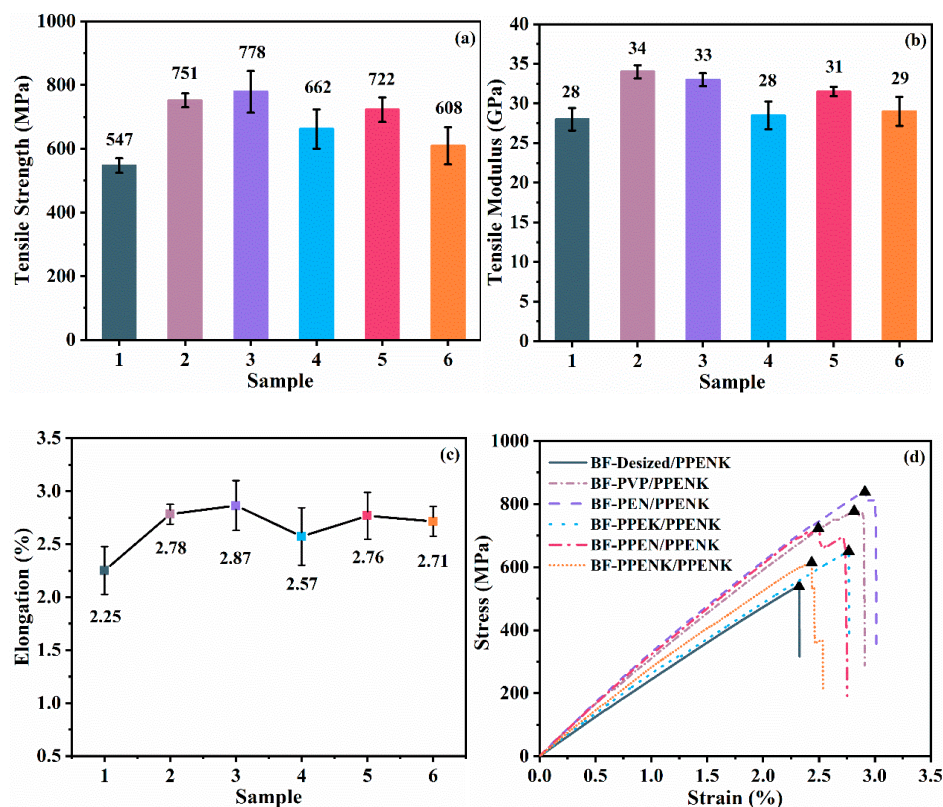


Figure 3. Tensile properties of the 1: BF—Desized/PPENK, 2: BF-PVP/PPENK, 3: BF-PEN/PPENK, 4: BF-PPEK/PPENK, 5: BF-PPEN/PPENK and 6: BF-PPENK/PPENK composites; (a) strength, (b) modulus, (c) breaking strain and (d) stress–strain curves.

3.5. Tensile Failure Mechanism

In the longitudinal tensile test of unidirectional composites, the damage expansion can be divided into four types: (1) interface debonding of the fiber and matrix; (2) the cracks in the fiber extend to the matrix; (3) the matrix deformation and ductile fracture; (4) sequential fracture of the adjacent fibers. Additionally, different damage expansion forms and processes will lead to three kinds of typical failure modes: (1) the bundle failing model; (2) the fracture failing model; (3) the accumulated damage model. Figure S6 displays the macro-morphologies of tensile failure modes for the resultant composites. On the whole, the tensile failure modes of all the BF/PPENK composites are the bundle failing model, which can be attributed to the poor tow-spreading condition of the BF bundles. However, their failure morphologies were different, and the number of cracks on the specimens had a certain positive correlation with the tensile strength. The BF—Desized/PPENK composite has the least cracks, which is related to its poor interfacial strength and the inferior wettability of the PPENK matrix on BF. In contrast, the resized BF/PPENK composites split into more fragments, due to their improved wettability of BF and interfacial properties. The SEM images reflected the much more microscopic failure mechanisms. As shown in Figure 4a, the surface of the pull-out fiber was smooth, which confirmed that the main failure mechanism of BF—Desized/PPENK was interface-debonding failure. For the BF-PVP/PPENK, BF-PPEK/PPENK and BF-PPENK/PPENK composites, the surface roughness and the resin content of the pull-out fiber surface were increased, but no obvious shear damage morphology appeared for the matrix (Figure 4b,d,f), indicating that the

cracks propagated along with the fiber in the interfacial phase. In this case, the tightly adhesive matrix on the BF surface can effectively transfer the load, resulting in improved tensile strength to a certain extent. As for the BF-PVP/PPENK composite, the significantly increased tensile strength may be related to the strong interfacial flexibility and polarity. In particular, BF-PEN/PPENK has the obvious “fish-scale” morphology (Figure 4c), and the main tensile-failure mechanisms were matrix deformation and ductile fracture, because of the strong interfacial adhesion. The mechanism of the BF-PPEN/PPENK composite is similar to that of BF-PEN/PPENK, but the matrix resin deformation is not obvious because of the relatively low number-average DP, weak polarity and rigid chain structures of PPEN.

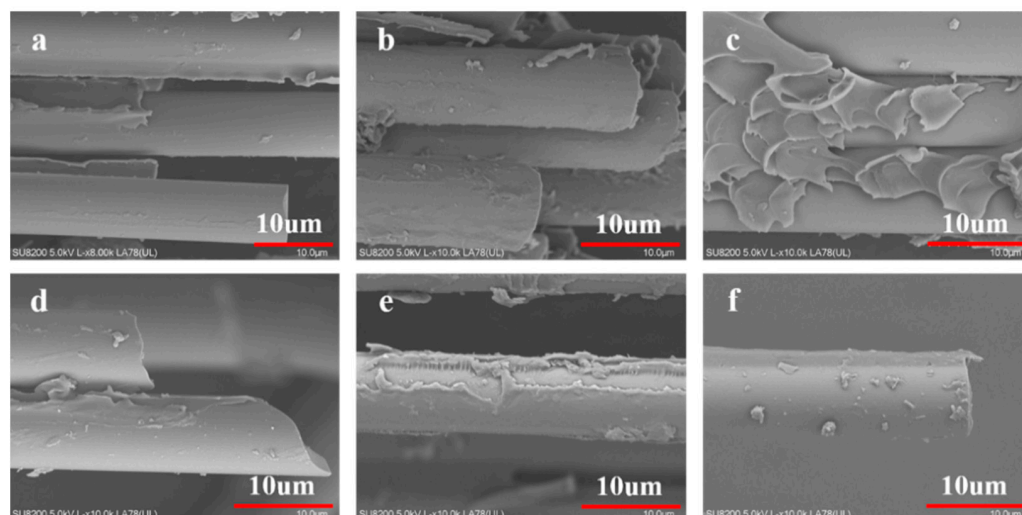


Figure 4. SEM images of tensile test fracture; (a) BF—Desized/PPENK, (b) BF-PVP/PPENK, (c) BF-PEN/PPENK, (d) BF-PPEK/PPENK, (e) BF-PPEN/PPENK and (f) BF-PPENK/PPENK composites.

3.6. Compressive Properties

The compressive properties of the BF/PPENK composites are shown in Figure 5. The compressive strength and modulus of the BF-PVP/PPENK composite were slightly increased to 489 MPa and 39 GPa compared with BF—Desized/PPENK (403 MPa and 34 GPa). This increase was less obvious than that of the tensile strength, probably due to the much smaller size and larger load of samples for the compressive test than those in the tensile test. That is, when the compression load reaches a very large level (more than 20 kN), the flexible interfacial phase is destroyed in a moment, and the ability of the flexible layer to retard crack propagation is greatly weakened, so the breaking strain of the BF-PVP/PPENK composite was decreased. Compared with the BF—Desized/PPENK, the compressive strengths of BF-PEN/PPENK and BF-PPEN/PPENK composites are 601 MPa and 694 MPa, increased by 49% and 72%, respectively. On the one hand, this may be related to the strong polar interaction of the cyano groups, resulting in the enhanced interfacial strength. On the other hand, the molecular chains of aromatic structures have strong rigidity and can withstand higher loads. Due to the stronger rigidity of the PPEN chain than the PEN chain, the modulus of BF-PPEN/PPENK (43 GPa) is higher than BF-PEN/PPENK (36 GPa), while the breaking strain of BF-PPEN/PPENK (2.04%) is lower than that of BF-PEN/PPENK (2.25%). This is also reflected in the compressive properties of the BF-PPEK/PPENK composite, whose strength, modulus and breaking strain are improved to 568 MPa, 40 GPa and 1.82%, respectively. The mildly enhanced compressive properties of BF-PPENK/PPENK composites mainly come from the improvement in wettability of the resized BF with PPENK. Owing to the rigid structure and low number-average DP of the PPENK sizing agent, its film-forming property is too poor to form a reasonable interfacial phase structure. On the whole, the appropriate content of the rigid structure in the sizing agent is necessary to endow the interfacial phase with a certain strength, which means that

the good film-forming ability and proper flexibility of the sizing agent are significant for the interfacial phase of BF-reinforced high-performance thermoplastic composites.

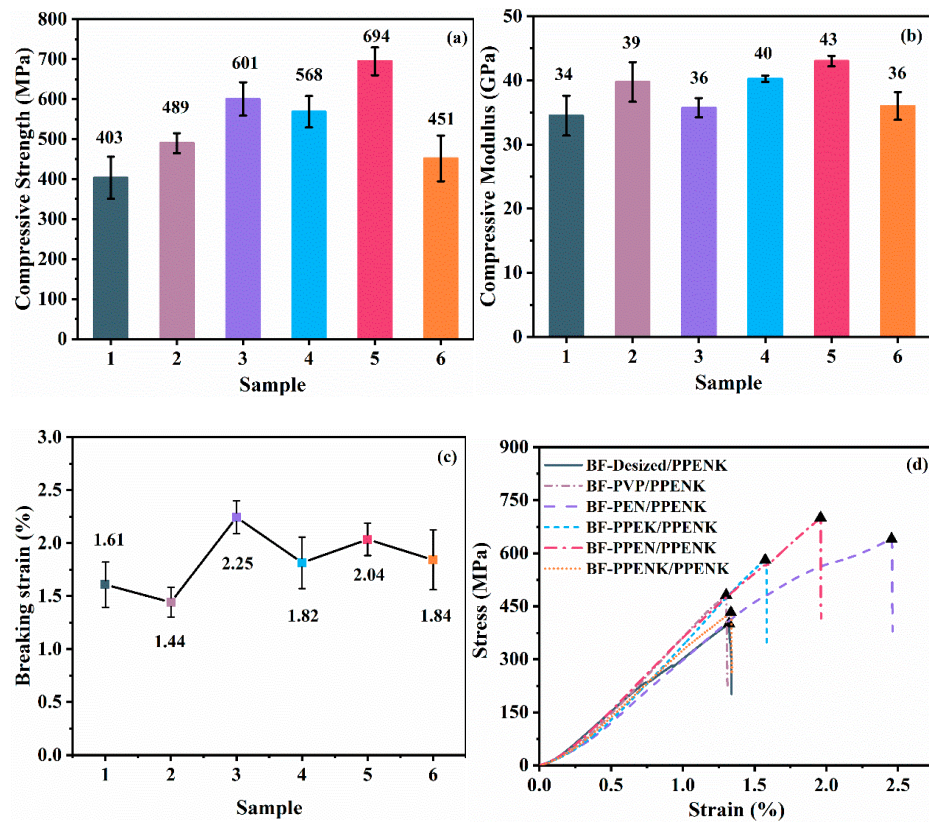


Figure 5. Compressive properties of the 1: BF—Desized/PPENK, 2: BF-PVP/PPENK, 3: BF-PEN/PPENK, 4: BF-PPEK/PPENK, 5: BF-PPEN/PPENK and 6: BF-PPENK/PPENK composites; (a) strength, (b) modulus, (c) breaking strain and (d) stress–strain curves.

In order to clarify the position of the BF/PPENK composites in the field of BFRP, and to highlight the advancement of this work, the tensile and compressive strengths were compared with those reported in references [44–48]. As shown in Figure 6, this work achieved good results compared with basalt-fiber-fabric-reinforced epoxy resin (BF/EP) composites.

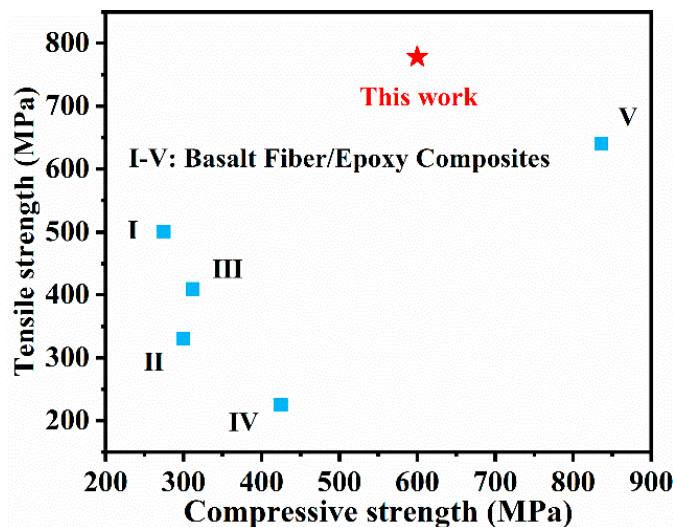


Figure 6. Comparison of tensile and compressive strength of BF-PEN/PPENK with BF/EP composites (I–V: [44–48]).

3.7. Compressive Failure Mechanism

The compressive failure modes of FRP composites are relatively complex, and the common forms include delamination, micro-buckling, shear fracture, kink band and bundle splitting [49,50]. Generally, the final compressive failure model of each composite laminate is a combination of them. Among the many influencing factors, fiber, matrix and interfacial phase structure are the most complex and critical [51]. Madhukar et al. [52] found that the compressive failure mechanism depended strongly on the interface conditions; that is, as the interfacial strength increased, and the compression failure mode changed from delamination and buckling to bundle splitting to fiber compressive failure.

As shown in Figure 7a, many interlaminar cracks appeared on the side of the BF—Desized/PPENK, and the cracks propagated between the layers along the direction of BF, which is a typical delamination failure mode, mainly due to the weak interfacial strength [50]. The broken ends of fiber bundles and brittle fracture for the BF-PVP/PPENK composite (Figure 7b) indicated that the bundle splitting was its main failure mode. This is because of the excessively flexible interfacial phase which is easily destroyed under the huge load, and the fiber bundles endure almost all the stress. When the weak links in the fibers are overload and fracture, the cracks rapidly expand to the surrounding fibers and cause the fiber bundles to bend and fracture, frequently accompanied by delamination. The obvious “V”-shaped fracture zone of the BF-PPEK/PPENK composite indicated that its main failure mode was shear fracture (Figure 7d), which is closely related to the strong rigid structures in the PPEK chains; due to this relatively rigid interfacial phase, it prevents the crack from propagating along the direction of fiber and eventually developed an inclined crack. The “Z”-shaped inclined band in the failure morphology of BF-PEN/PPENK was a kink band (Figure 7c), implying the improved interfacial properties, and its formation is mainly caused by the micro-buckling of the fibers. The kink band was also observed on the BF-PPEN/PPENK and BF-PPENK/PPENK composites (Figure 7e,f), but there was another failure mode of shear fracture in the former, which may be attributed to the much better interfacial properties of BF-PPEN/PPENK.

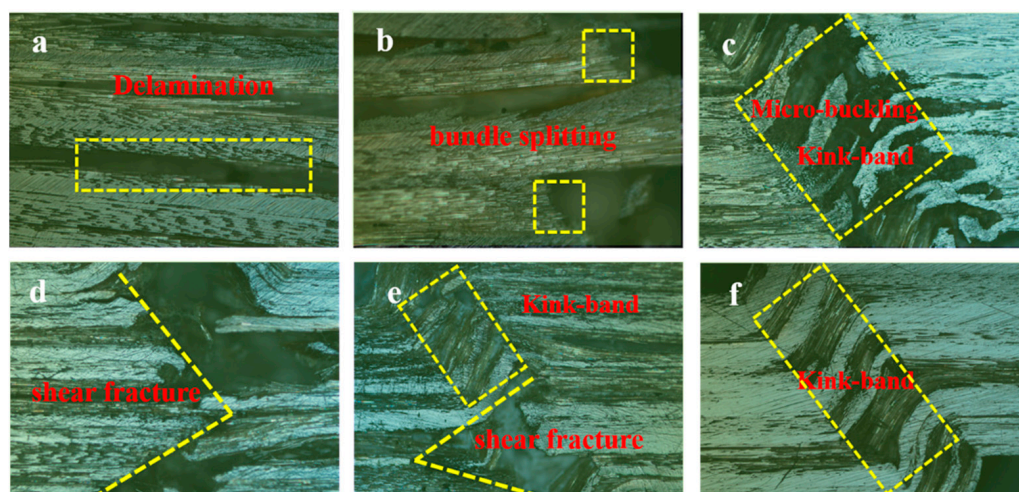


Figure 7. Optical microscope photographs of compression failure sample; (a) BF—Desized/PPENK, (b) BF-PVP/PPENK, (c) BF-PEN/PPENK, (d) BF-PPEK/PPENK, (e) BF-PPEN/PPENK and (f) BF-PPENK/PPENK composites.

The SEM images indicated that the delamination of the BF—Desized/PPENK composites has a smooth surface, which means that the adhesion between the fibers and matrix is weak (Figure 8a). Compressive failure microtopography of the BF-PVP/PPENK and BF-PPEK/PPENK composites showed no fiber fragments on the delaminated surface and a little plastic deformation (Figure 8b,d), but the compressive strength of the latter was higher than the former. This further confirms that the sizing agent with rigid chain structures has a great effect on the improvement in the compressive properties. Particularly, the

abundant BF fragments in Figure 8c,e demonstrated that PEN and PPEN sizing agents were more effective than others in improving the compressive performance of BF/PPENK composites because of the cyano groups and the aromatic rings contained in the molecular chains. Moreover, the compressive strengths of BF-PEN/PPENK and BF-PPEN/PPENK composites were much higher than others, which are attributed to energy dissipation by the fiber crushing. However, even though the BF-PPENK/PPENK compression failure mode was kink band, it did not have many fiber fragments, which can be interpreted as a result of its relatively low compressive properties (Figure 8f).

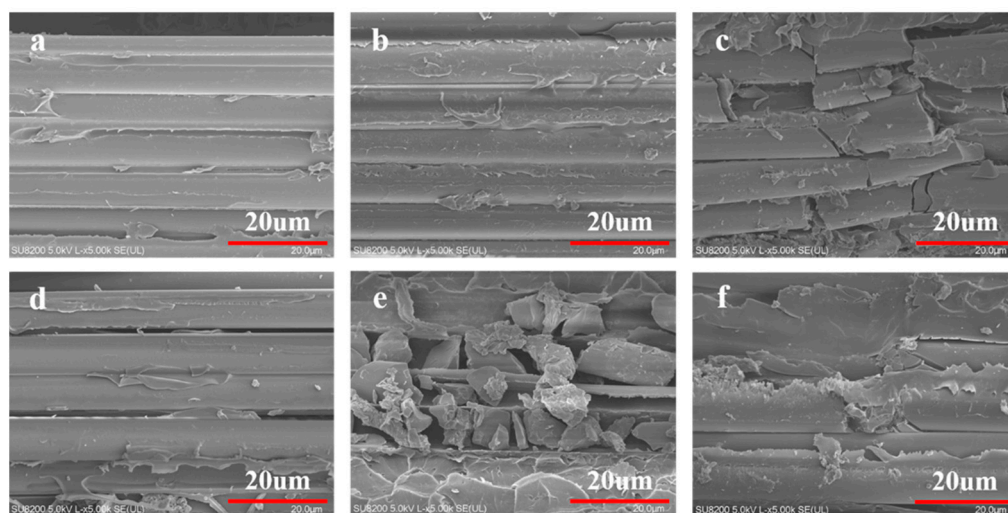


Figure 8. SEM images of compression failure sample; (a) BF—Desized/PPENK, (b) BF-PVP/PPENK, (c) BF-PEN/PPENK, (d) BF-PPEK/PPENK, (e) BF-PPEN/PPENK and (f) BF-PPENK/PPENK composites.

3.8. Flexural Strength and ILSS

The flexural strengths of BF-PEN/PPENK and BF-PPEN/PPENK composites were 1114 MPa and 1094 MPa, increased by 20% and 18% compared with BF—Desized/PPENK (927 MPa), respectively (Figure 9a). However, the flexural strengths of BF-PVP/PPENK, BF-PPEK/PPENK and BF-PPENK/PPENK composites were slightly decreased. The interlaminar shear strength (ILSS) can largely reflect the interfacial properties of the composite [53], and the ILSS of BF-PVP/PPENK, BF-PEN/PPENK, BF-PPEK/PPENK, BF-PPEN/PPENK and BF-PPENK/PPENK composites reached 50 MPa, 57 MPa, 52 MPa, 54 MPa, and 51 MPa, which were increased by 13.6%, 29.5%, 18.2%, 22.7%, and 15.9%, respectively (Figure 9b). Therefore, compared with the other four sizing agents, PEN and PPEN are more effective in improving the interfacial properties of the BF/PPENK composites, while the flexible interfacial phase structures constructed by PVP, PPEK and PPENK are not very reasonable. In fact, the flexible interfacial layer has two effects on the mechanical properties of the composite. On the one hand, it can improve the interfacial properties by deformation; on the other hand, the low modulus will reduce the strength. However, when the improvement is not enough to compensate for the weakening, the composite exhibits a decrease in strength. Especially, when the composite is subjected to a bending test, it will be subjected to a variety of forces such as tension, compression and shear, and the effect of the resultant force will make this influence more obvious.

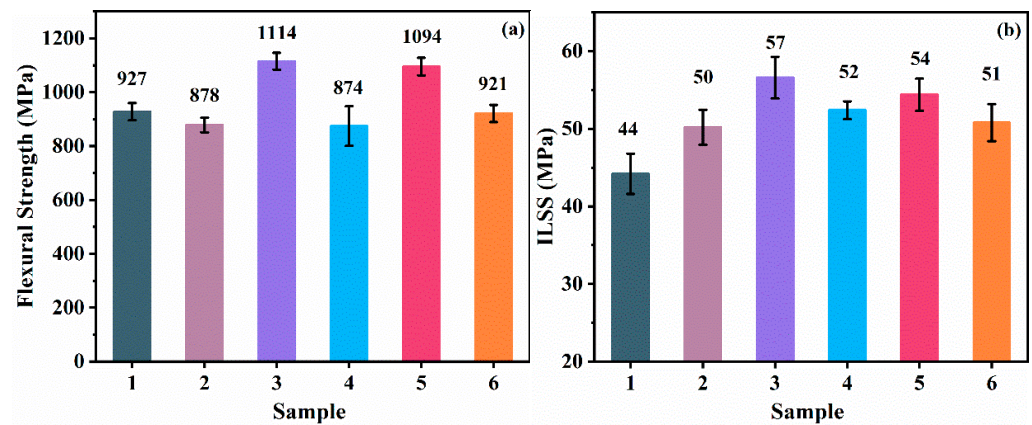


Figure 9. (a) Flexural strength and (b) interlaminar shear strength of the 1: BF—Desized/PPENK, 2: BF-PVP/PPENK, 3: BF-PEN/PPENK, 4: BF-PPEK/PPENK, 5: BF-PPEN/PPENK and 6: BF-PPENK/PPENK composites.

4. Conclusions

In this work, five sizing agents (PVP, PEN, PPEK, PPEN and PPENK) were successfully coated on the BF surface to improve the interfacial and mechanical properties of the BF/PPENK composites. The PVP sizing agent can form a flexible interfacial phase with enhanced mechanical properties in BF/PPENK composites, while the BF-PEN/PPENK composite with the PEN sizing agent has the strongest interfacial phase due to the relatively rigid chain structures, and strong polar interaction, π - π interaction and compatibility of PEN with the PPENK matrix, resulting in the even higher T_g and mechanical properties. Furthermore, for the other three composites with the similar sizing agents containing a phthalazinone structure, BF-PPEN/PPENK exhibited higher tensile strength, tensile modulus and elongation at break than those of BF-PPEK/PPENK and BF-PPENK/PPENK, due to the relatively better film-forming properties and many more polar cyano groups ($-\text{CN}$) of PPEN than those of PPEK and PPENK. In summary, thermoplastic sizing agents with favorable film-forming ability on BF, good compatibility with the matrix, moderate flexibility and strong polar group are preferred for BF-reinforced high-performance thermoplastic composites with improved interfacial and mechanical properties.

Supplementary Materials: The following are available online at <https://www.mdpi.com/article/10.3390/polym14142947/s1>. Figure S1 TGA curves of the sizing agents of PVP, PEN, PPEK, PPEN and PPENK. Figure S2 Synthesis of LMW PEN. Figure S3 The preparation process flow diagram of composite laminates. Figure S4 XPS spectra of the desized and re-sized basalt fibers; (a) survey scan spectra and (b) narrow scan spectra in the N 1s regions. Figure S5 Loss modulus and $\tan \delta$ curves of BF-Desized/PPENK, BF-PVP/PPENK, BF-PEN/PPENK, BF-PPEK/PPENK, BF-PPEN/PPENK and BF-PPENK/PPENK composites. Figure S6 Images of overall morphology of tensile failure; (a) BF-Desized/PPENK, (b) BF-PVP/PPENK, (c) BF-PEN/PPENK, (d) BF-PPEK/PPENK, (e) BF-PPEN/PPENK and (f) BF-PPENK/PPENK composites. Figure S7 Flexural modulus of the 1: BF-Desized/PPENK, 2: BF-PVP/PPENK, 3: BF-PEN/PPENK, 4: BF-PPEK/PPENK, 5: BF-PPEN/PPENK and 6: BF-PPENK/PPENK composites. Table S1 Tensile and compression tests of BF/PPENK composites. Table S2 Quantification of the atomic chemical composition of the BFs. Table S3 DMA test results of BF/PPENK composites. Table S4 Tensile and compression tests of BF/PPENK composites. Table S5 Flexural and ILSS tests of BF/PPENK composites.

Author Contributions: H.J.: Writing—original draft, Data curation. C.L.: Investigation, Supervision, Funding acquisition. Y.Q.: Review and revision. Y.Z.: Review and editing. K.F.: Formal analysis. M.Z.: Revised writing. X.J.: Supervision. All authors have read and agreed to the published version of the manuscript.

Funding: This research was funded by the National Natural Science Foundation of China (91860204) and the Fundamental Research Funds for the Central Universities (DUT20LAB305 and DUT20TD114).

Institutional Review Board Statement: Not applicable.

Informed Consent Statement: Not applicable.

Data Availability Statement: Not applicable.

Conflicts of Interest: The authors declare no conflict of interest.

References

1. Xu, J.; Xia, L.; Luo, J.; Lu, S.; Huang, X.; Zhong, B.; Zhang, T.; Wen, G.; Wu, X.; Xiong, L.; et al. High-Performance Electromagnetic Wave Absorbing CNT/SiCf Composites: Synthesis, Tuning, and Mechanism. *ACS Appl. Mater. Interfaces* **2020**, *12*, 20775–20784. [[CrossRef](#)] [[PubMed](#)]
2. Gao, S.-l.; Zhuang, R.-C.; Zhang, J.; Liu, J.-W.; Mäder, E. Glass Fibers with Carbon Nanotube Networks as Multifunctional Sensors. *Adv. Funct. Mater.* **2010**, *20*, 1885–1893. [[CrossRef](#)]
3. Lin, F.; Du, X.; Li, W.; Jiang, J.; Chen, N. Interfacial properties of high failure strain polyimide fiber/epoxy composites analyzed by a modified single fiber fragmentation test. *Appl. Surf. Sci.* **2020**, *513*, 145869. [[CrossRef](#)]
4. Li, C.; Shi, Y.; Zhang, R.; Wang, G.; Jia, J. Effect of surface modifications on the properties of UHMWPE fibres and their composites. *e-Polymers* **2019**, *19*, 40–49. [[CrossRef](#)]
5. Ramezani-pour, A.A.; Esmaeili, M.; Ghahari, S.A.; Najafi, M.H. Laboratory study on the effect of polypropylene fiber on durability, and physical and mechanical characteristic of concrete for application in sleepers. *Constr. Build. Mater.* **2013**, *44*, 411–418. [[CrossRef](#)]
6. Bulut, M.; Bozkurt, O.Y.; Erklig, A.; Yaykasli, H.; Ozbek, O. Mechanical and Dynamic Properties of Basalt Fiber-Reinforced Composites with Nanoclay Particles. *Arab. J. Sci. Eng.* **2020**, *45*, 1017–1033. [[CrossRef](#)]
7. Kizilkanat, A.B.; Kabay, N.; Akyüncü, V.; Chowdhury, S.; Akça, A.H. Mechanical properties and fracture behavior of basalt and glass fiber reinforced concrete: An experimental study. *Constr. Build. Mater.* **2015**, *100*, 218–224. [[CrossRef](#)]
8. Jayasuriya, S.; Chegeni, B.; Das, S. Use of BFRP wrap for rehabilitation of pipeline in bending with various corrosion depths. *J. Pipeline Syst. Eng. Pract.* **2020**, *11*, 04019038. [[CrossRef](#)]
9. Zhang, M.; Denning, R.; Zhong, Z.; Wang, X.; Shen, Y.; Naebe, M. Investigation of heat transfer properties of plasma-treated and silicone-elastomer coated basalt fabric. *Coatings* **2019**, *9*, 292. [[CrossRef](#)]
10. Monaldo, E.; Nerilli, F.; Vairo, G. Basalt-based fiber-reinforced materials and structural applications in civil engineering. *Compos. Struct.* **2019**, *214*, 246–263. [[CrossRef](#)]
11. Hao, B.; Förster, T.; Mäder, E.; Ma, P. Modification of basalt fibre using pyrolytic carbon coating for sensing applications. *Compos. Part A Appl. Sci. Manuf.* **2017**, *101*, 123–128. [[CrossRef](#)]
12. Simone, B.; Giuseppe, D.C.; Natalino, D.B.; Carosena, M.; Giovanni, M.C.; Ernesto, M.; Pietro, R.; Giorgio, S. Lock-in thermography and ultrasonic testing of impacted basalt fibers reinforced thermoplastic matrix composites. *Appl. Sci.* **2019**, *9*, 3025. [[CrossRef](#)]
13. Kim, D.; Mittal, G.; Kim, M.; Kim, S.; Yop Rhee, K. Surface modification of MMT and its effect on fatigue and fracture behavior of basalt/epoxy based composites in a seawater environment. *Appl. Surf. Sci.* **2019**, *473*, 55–58. [[CrossRef](#)]
14. Liu, S.; Wu, G.; Yu, J.; Chen, X.; Guo, J.; Zhang, X.; Wang, P.; Yin, X. Surface modification of basalt fiber (BF) for improving compatibilities between BF and poly lactic acid (PLA) matrix. *Compos. Interfaces* **2018**, *26*, 275–290. [[CrossRef](#)]
15. Xie, J.-H.; Wei, M.-W.; Huang, P.-Y.; Zhang, H.; Chen, P.-S. Fatigue behavior of the basalt fiber-reinforced polymer/concrete interface under wet-dry cycling in a marine environment. *Constr. Build. Mater.* **2019**, *228*, 117065. [[CrossRef](#)]
16. Khandelwal, S.; Rhee, K.Y. Recent advances in basalt-fiber-reinforced composites: Tailoring the fiber-matrix interface. *Compos. Part B Eng.* **2020**, *192*, 108011. [[CrossRef](#)]
17. Guo, H.; Zhan, Y.; Chen, Z.; Meng, F.; Wei, J.; Liu, X. Decoration of basalt fibers with hybrid Fe₃O₄ microspheres and their microwave absorption application in bisphthalonitrile composites. *J. Mater. Chem. A* **2013**, *1*, 2286–2296. [[CrossRef](#)]
18. Li, Z.; Wan, J.; Li, Y.; Li, Y.; Zhao, F.; Zhao, S. Effects of coupling agents on the properties of an NR/SBR matrix and its adhesion to continuous basalt fiber cords. *J. Appl. Polym. Sci.* **2018**, *136*, 47098. [[CrossRef](#)]
19. Yang, W.; Zhang, Y.R.; Yuen, A.C.Y.; Chen, T.B.Y.; Chan, M.C.; Peng, L.Z.; Yang, W.J.; Zhu, S.E.; Yang, B.H.; Hu, K.H.; et al. Synthesis of phosphorus-containing silane coupling agent for surface modification of glass fibers: Effective reinforcement and flame retardancy in poly(1,4-butylene terephthalate). *Chem. Eng. J.* **2017**, *321*, 257–267. [[CrossRef](#)]
20. Yuan, X.; Jiang, J.; Wei, H.; Yuan, C.; Wang, M.; Zhang, D.; Liu, L.; Huang, Y.; Gao, G.; Jiang, Z. PAI/MXene sizing-based dual functional coating for carbon fiber/PEEK composite. *Compos. Sci. Technol.* **2021**, *201*, 108496. [[CrossRef](#)]
21. Xiang, Y.; Xie, Y.; Long, G. Effect of basalt fiber surface silane coupling agent coating on fiber-reinforced asphalt: From macro-mechanical performance to micro-interfacial mechanism. *Constr. Build. Mater.* **2018**, *179*, 107–116. [[CrossRef](#)]
22. Zhang, S.; Liu, W.; Wang, J.; Li, B.; Hao, L.; Wang, R. Improvement of interfacial properties of carbon fiber-reinforced poly(phthalazinone ether ketone) composites by introducing carbon nanotube to the interphase. *Polym. Compos.* **2015**, *36*, 26–33. [[CrossRef](#)]

23. Thomason, J.L.; Adzima, L.J. Sizing up the interphase: An insider's guide to the science of sizing. *Compos. Part A Appl. Sci. Manuf.* **2001**, *32*, 313–321. [[CrossRef](#)]
24. Dong, Y.; Zhu, Y.; Zhao, Y.; Liu, F.; Wang, E.; Fu, Y. Enhance interfacial properties of glass fiber/epoxy composites with environment-friendly water-based hybrid sizing agent. *Compos. Part A Appl. Sci. Manuf.* **2017**, *102*, 357–367. [[CrossRef](#)]
25. Chen, Z.; Huang, Y. Preparation and performance of fumed silica-stabilized epoxy resin pickering emulsion for basalt fiber-sizing agents. *Adv. Compos. Hybrid Mater.* **2021**, *4*, 1205–1214. [[CrossRef](#)]
26. Hassan, E.A.M.; Yang, L.; Elagib, T.H.H.; Ge, D.; Lv, X.; Zhou, J.; Yu, M.; Zhu, S. Synergistic effect of hydrogen bonding and π - π stacking in interface of CF/PEEK composites. *Compos. Part B Eng.* **2019**, *171*, 70–77. [[CrossRef](#)]
27. Bowman, S.; Jiang, Q.; Memon, H.; Qiu, Y.; Liu, W.; Wei, Y. Effects of styrene-acrylic sizing on the mechanical properties of carbon fiber thermoplastic towpregs and their composites. *Molecules* **2018**, *23*, 547. [[CrossRef](#)]
28. Giraud, I.; Franceschi, S.; Perez, E.; Lacabanne, C.; Dantras, E. Influence of new thermoplastic sizing agents on the mechanical behavior of poly(ether ketone ketone)/carbon fiber composites. *J. Appl. Polym. Sci.* **2015**, *132*, 1–5. [[CrossRef](#)]
29. Liu, L.; Yan, F.; Li, M.; Zhang, M.; Xiao, L.; Shang, L.; Ao, Y. A novel thermoplastic sizing containing graphene oxide functionalized with structural analogs of matrix for improving interfacial adhesion of CF/PES composites. *Compos. Part A Appl. Sci. Manuf.* **2018**, *114*, 418–428. [[CrossRef](#)]
30. Kodokian, G.K.A.; Kinloch, A.J. Surface pretreatment and adhesion of thermoplastic fibre-composites. *J. Mater. Sci. Lett.* **1988**, *7*, 625–627. [[CrossRef](#)]
31. Zhu, S.; Qian, Y.; Hassan, E.A.M.; Shi, R.; Yang, L.; Cao, H.; Zhou, J.; Ge, D.; Yu, M. Enhanced interfacial interactions by PEEK-grafting and coupling of acylated CNT for GF/PEEK composites. *Compos. Commun.* **2020**, *18*, 43–48. [[CrossRef](#)]
32. Wang, X.; Huang, Z.; Lai, M.; Jiang, L.; Zhang, Y.; Zhou, H. Highly enhancing the interfacial strength of CF/PEEK composites by introducing PAIK onto diazonium functionalized carbon fibers. *Appl. Surf. Sci.* **2020**, *510*, 145400. [[CrossRef](#)]
33. Hassan, E.A.M.; Ge, D.; Yang, L.; Zhou, J.; Liu, M.; Yu, M.; Zhu, S. Highly boosting the interlaminar shear strength of CF/PEEK composites via introduction of PEKK onto activated CF. *Compos. Part A Appl. Sci. Manuf.* **2018**, *112*, 155–160. [[CrossRef](#)]
34. Wang, T.; Jiao, Y.; Mi, Z.; Li, J.; Wang, D.; Zhao, X.; Zhou, H.; Chen, C. PEEK composites with polyimide sizing SCF as reinforcement: Preparation, characterization, and mechanical properties. *High Perform. Polym.* **2019**, *32*, 383–393. [[CrossRef](#)]
35. Li, X.; Meng, Y.; Jian, X.; Hay, A. Synthesis and properties of copoly(ether ketone) containing hydroquinone and phthalazinone moieties. *Polym. Mater. Sci. Eng.* **1998**, *14*, 37–39. [[CrossRef](#)]
36. Wang, M.; Liu, C.; Liu, Z.; Dong, L.; Jian, X. Synthesis and characterization of phthalazinone-containing poly (aryl ether nitrile ketone)s. *Acta Polym. Sin.* **2007**, *09*, 833–837. [[CrossRef](#)]
37. Kim, M.T.; Kim, M.H.; Rhee, K.Y.; Park, S.J. Study on an oxygen plasma treatment of a basalt fiber and its effect on the interlaminar fracture property of basalt/epoxy woven composites. *Compos. Part B Eng.* **2011**, *42*, 499–504. [[CrossRef](#)]
38. Yu, S.; Oh, K.H.; Hwang, J.Y.; Hong, S.H. The effect of amino-silane coupling agents having different molecular structures on the mechanical properties of basalt fiber-reinforced polyamide 6,6 composites. *Compos. Part B Eng.* **2019**, *163*, 511–521. [[CrossRef](#)]
39. Zhang, J.; Li, Y.; Xing, D.; Wang, Q.; Wang, H.; Koubaa, A. Reinforcement of continuous fibers for extruded wood-flour/HDPE composites: Effects of fiber type and amount. *Constr. Build. Mater.* **2019**, *228*, 116718. [[CrossRef](#)]
40. Gangineni, P.K.; Yandrapu, S.; Ghosh, S.K.; Anand, A.; Prusty, R.K.; Ray, B.C. Mechanical behavior of Graphene decorated carbon fiber reinforced polymer composites: An assessment of the influence of functional groups. *Compos. Part A Appl. Sci. Manuf.* **2019**, *122*, 36–44. [[CrossRef](#)]
41. Murayama, T.; Lawton, E.L. Dynamic loss energy measurement of tire cord adhesion to rubber. *J. Appl. Polym. Sci.* **1973**, *17*, 669–677. [[CrossRef](#)]
42. Jia, H.; Liu, C.; Qiao, Y.; Zhang, Y.; Dang, X.; Chen, Y.; Jian, X. Enhanced interfacial and mechanical properties of basalt fiber reinforced poly(aryl ether nitrile ketone) composites by amino-silane coupling agents. *Polymer* **2021**, *230*, 124028. [[CrossRef](#)]
43. Chauhan, S.; Karmarkar, A.; Aggarwal, P. Damping behavior of wood filled polypropylene composites. *J. Appl. Polym. Sci.* **2009**, *114*, 2421–2426. [[CrossRef](#)]
44. Lopresto, V.; Leone, C.; De Iorio, I. Mechanical characterisation of basalt fibre reinforced plastic. *Compos. Part B Eng.* **2011**, *42*, 717–723. [[CrossRef](#)]
45. Chairman, C.A.; Kumaresh Babu, S.P. Mechanical and abrasive wear behavior of glass and basalt fabric-reinforced epoxy composites. *J. Appl. Polym. Sci.* **2013**, *130*, 120–130. [[CrossRef](#)]
46. Colombo, C.; Vergani, L.; Burman, M. Static and fatigue characterisation of new basalt fibre reinforced composites. *Compos. Struct.* **2012**, *94*, 1165–1174. [[CrossRef](#)]
47. Varley, R.J.; Tian, W.; Leong, K.H.; Leong, A.Y.; Fredo, F.; Quaresimin, M. The effect of surface treatments on the mechanical properties of basalt-reinforced epoxy composites. *Polym. Compos.* **2013**, *34*, 320–329. [[CrossRef](#)]
48. Wang, M.; Zhang, Z.; Li, Y.; Li, M.; Sun, Z. Chemical Durability and Mechanical Properties of Alkali-proof Basalt Fiber and its Reinforced Epoxy Composites. *J. Reinf. Plast. Compos.* **2008**, *27*, 393–407. [[CrossRef](#)]
49. Williams, T.O.; Cairns, D.S. A model for the compressive failure of composite materials. *J. Compos. Mater.* **1994**, *28*, 92–111. [[CrossRef](#)]
50. Narayanan, S.; Schadler, L.S. Mechanisms of kink-band formation in graphite/epoxy composites: A micromechanical experimental study. *Compos. Sci. Technol.* **1999**, *59*, 2201–2213. [[CrossRef](#)]

51. De Carvalho, N.V.; Pinho, S.T.; Robinson, P. An experimental study of failure initiation and propagation in 2D woven composites under compression. *Compos. Sci. Technol.* **2011**, *71*, 1316–1325. [[CrossRef](#)]
52. Madhukar, M.S.; Drzal, L.T. Fiber-matrix adhesion and its effect on composite mechanical properties. III. Longitudinal (0°) compressive properties of graphite/epoxy composites. *J. Compos. Mater.* **1992**, *26*, 310–333. [[CrossRef](#)]
53. Bader, M.G.; Bailey, J.E.; Bell, I. The effect of fibre-matrix interface strength on the impact and fracture properties of carbon-fibre reinforced epoxy resin composites. *J. Phys. D Appl. Phys.* **1973**, *6*, 572–586. [[CrossRef](#)]